47th AIAA/ASME/SAE/ASEE Joint Propulsion Conference & Exhibit
31 July - 03 August 2011, San Diego, California

AIAA 2011-5781

Cavitation and Flow Instabilities in a 4-Bladed Axial Inducer Designed by Means of a Reduced Order Analytical Model

Angelo Cervone[1], Lucio Torre[2], Angelo Pasini[3] and Luca d'Agostino[4]

ALTA S.p.A. - Via Gherardesca, 5 - 56121 Ospedaletto, Pisa, Italy

The paper illustrates the results of an experimental campaign conducted at Alta S.p.A. in the CPRTF (Cavitating Pump Rotordynamic Test Facility). Tests have been carried out in water on the four-bladed DAPAMITO4 inducer, designed and manufactured by means of a reduced-order model developed at Alta S.p.A., at several values of the flow coefficient and the water temperature. Several non-synchronous instabilities have been observed on the inducer, including an axial surge, a backflow oscillation and, at higher temperatures, an incipient rotating cavitation and a backflow vortices instability. In addition, a synchronous rotating cavitation (also leading to the characteristic "one step" shape of the cavitating performance curve near to head breakdown conditions) has been detected at all the investigated flow conditions, and the amplitude of oscillations associated to this instability generally tends to decrease at higher water temperatures.

Nomenclature

$A\%$	amplitude of oscillations (expressed as % of the maximum value)
$c_{\%}$	tip clearance/mean blade height ratio
n	number of lobes
p_{in}	inlet static pressure [Pa]
p_V	vapor pressure [Pa]
Q	volumetric flow rate [m^3/s]
r_T	inducer tip radius [m]
T	water temperature [°C]
α	incidence angle
β_b	blade angle evaluated w.r.t. the azimuthal direction [rad]
γ_{xy}	coherence function
Δp	static pressure rise across the inducer [Pa]
Δp_t	total pressure rise [Pa]
$\Delta\theta$	angular spacing between the transducers [rad]
η	hydraulic efficiency $\eta = Q\,\Delta p_t / (\tau\,\Omega)$
σ	cavitation number $\sigma = (p_{in} - p_V) / 0.5\rho\Omega^2 r_T^2$
τ	torque [Nm]
φ	phase of the cross-spectrum [rad]

[1] Project Manager, ALTA S.p.A., Pisa, Italy, AIAA Member; a.cervone@alta-space.com
[2] Project Manager, ALTA S.p.A., Pisa, Italy, AIAA Member; l.torre@alta-space.com
[3] Project Engineer, ALTA S.p.A., Pisa, Italy, AIAA Member; a.pasini@alta-space.com
[4] Professor, Aerospace Engineering, Pisa University - Vice President, ALTA S.p.A., Pisa, Italy, AIAA Member; luca.dagostino@ing.unipi.it

Φ	flow coefficient $\Phi = Q/\pi\Omega r_T^3$
Φ_D	design flow coefficient
ρ	liquid density [kg/m^3]
Ψ	static head coefficient $\Psi = (\Delta p)/\rho\Omega^2 r_T^2$
Ω	inducer rotational speed [rad/s]

I. Introduction

IN the axial inducers used for liquid propellant rocket turbopumps, typically working under cavitating conditions, it is usual to observe the development of flow instabilities, which can seriously degrade the performance of the machine or even cause its rapid failure[1,2].

The cavitating behavior of a rotating machine can be related, at least to some extent, to that of a static cascade of hydrofoils; the first step for understanding cavitation instabilities in inducers is therefore typically represented by experimentation on test bodies in hydrodynamic tunnels. The onset of cavitation instabilities in 2-D hydrofoils is strongly related to the mean cavity length, which shows a strong dependence on the well known σ/α parameter (cavitation number divided to incidence angle)[3,4]. One of the most studied instabilities in hydrofoils is the so-called cloud cavitation, which consists in violent periodical fluctuations of the cavity length, typically occurring at constant Strouhal numbers and followed by the release of a cavity cloud at the conclusion of each cycle[5]. The nature of this form of instability in cavitating hydrofoils has been studied in detail[6], proving the correlation between cloud cavitation and the formation of a re-entrant jet at the cavity closure as a result of a critical adverse pressure gradient observed for cavity lengths greater than about 50% of chord[7,8,9].

Another driving parameter in the development of cavitation induced flow instabilities in 2-D cascades is the dimension of the cavity with respect to the thickness of the blade passage. In rotating cascades, the blockage induced by cavitation can lead to rotating instabilities similar to rotating stall in compressors, such as rotating cavitation[10,11,12,13] and rotating choke[14,15]. In particular, it has been found that the onset point of rotating cavitation corresponds to a cavity length equal to about 70% of blade spacing and, furthermore, that 4-bladed inducers are expected to show higher rotating cavitation frequency than 3-bladed inducers[16].

Finally, the presence of the blade tip and the consequent clearance between the impeller and the casing introduces further complexities in the development of cavitation and cavitation induced instabilities. The so-called backflow vortex cavitation, a rotating instability with multiple cells formed in backflow vortices, was detected for the first time in 1997 for two separated ranges of values of the cavitation number: at high cavitation numbers (3-4 times the breakdown cavitation number), when the tip vortex cavitation is the principal form of cavitation, and around the head breakdown for lower flow coefficients, where the backflow is particularly strong[17]. It has been recently shown that the extent of the cavitation backflow and, consequently, of the surge instability associated to it, can be significantly reduced by adding a "backflow restriction step" to the inducer casing[18].

It is well known that the noncavitating performance of inducers is relatively insensitive to the tip clearance for clearance/mean blade height ratios lower than 2%, but tends to rapidly degrade for larger values of this parameter. In addition, tip clearance affects the cavitation inception number in unshrouded machines since cavitation usually begins in the vortices associated to the tip clearance flows[19,20]. Finally, azimuthal instabilities like rotating cavitation are significantly influenced by the tip clearance, due to their strict correlation with the extent and characteristics of the tip vortices. The techniques proposed so far for suppressing rotating cavitation include: use of special custom-designed devices[21], modifications of the inlet housing[22], introduction of an axial groove along the inducer casing[23], cutbacks of the leading edges of alternate blades[24,25], design modifications of both inducer and inlet geometry[26].

The present paper illustrates the main results of an experimental campaign conducted using the CPRTF (Cavitating Pump Rotordynamic Test Facility) at Alta S.p.A. The tests have been carried out on the DAPAMITO4 inducer, a four-bladed axial pump designed and manufactured using a reduced-order analytical model for the prediction of geometry and noncavitating performance of typical space rocket inducers[27,28]. Experiments have been performed at different water temperatures and flow coefficients, under cavitating and noncavitating conditions, and the development of both rotating and longitudinal flow instabilities has been observed. The results of a similar test campaign conducted on a 3-bladed inducer, including in particular a detailed study of the influence of the blade tip clearance on the pump performance and the flow instabilities, have already been presented in a previous paper by the same authors[29].

II. Experimental Apparatus

A. Test Facility and Instrumentation

The Cavitating Pump Rotordynamic Test Facility (CPRTF, Figure 1) is a versatile and easily instrumentable facility operating in water[30], at temperatures up to 90 °C. The facility is intended as a flexible apparatus that can readily be adapted to conduct experimental investigations on virtually any kind of fluid dynamic phenomena relevant to high performance turbopumps in a wide variety of alternative configurations (impeller with axial, radial or mixed flow, with or without an inducer). The CPRTF has been especially designed for the analysis of unsteady flow phenomena and rotordynamic impeller forces in scaled cavitation tests under fluid dynamic and thermal cavitation similarity conditions. It can also be configured as a small water tunnel to be used for thermal cavitation tests aimed at fundamental investigations and/or experimental validation of numerical tools and simulations.

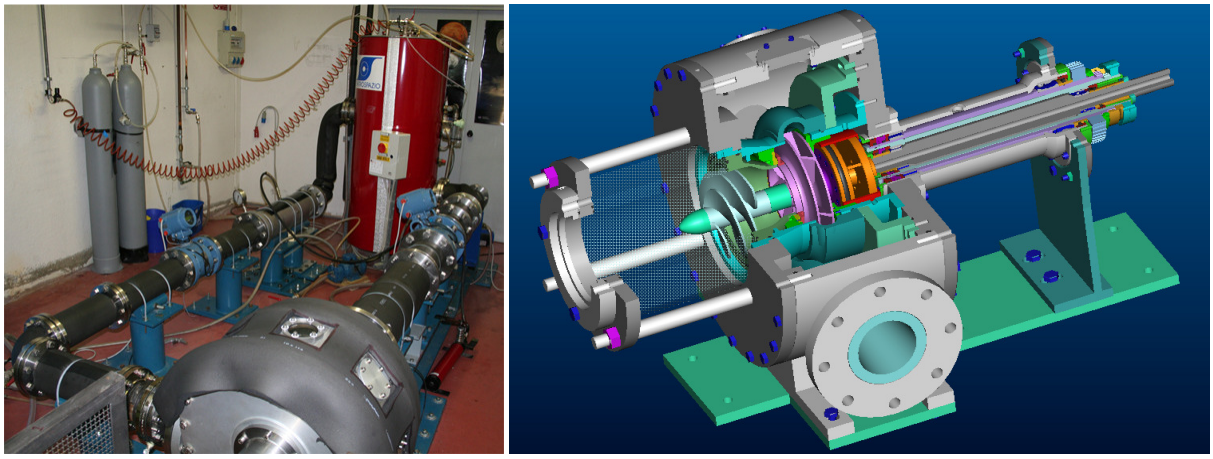

Figure 1. The Cavitating Pump Rotordynamic Test Facility (left) and cut-off drawing of the CPRTF test section (right).

The test section (Figure 1, right) can be equipped with a rotating dynamometer, for the measurement of the instantaneous forces and moments acting on the impeller, and with a mechanism capable of adjusting and rotating the eccentricity of the impeller axis in the range from 0 to 2 mm and ±3000 rpm for rotordynamic experiments. The inlet section, made in transparent Plexiglas, allows for multilateral optical access to the inducer flow. It can be instrumented with several flush-mounted piezoelectric pressure transducers (PCB M112A22, ICP® voltage mode-type, 0.1% class), located at different axial stations (Figure 2, in particular, shows the transducers installed at the inducer inlet and the blade tip). At each station, up to eight transducers can be mounted with a given angular spacing, in order to cross-correlate their signals for amplitude, phase and coherence analyses. As a result, waterfall plots of the power spectral density of the pressure fluctuations can be obtained as functions of the cavitation number, in order to identify the presence of instabilities in the flow conditions under consideration. Cross-correlation of two pressure signals from different locations allows for determining the axial or azimuthal nature of a given instability and, in the second case, the number of rotating cells involved.

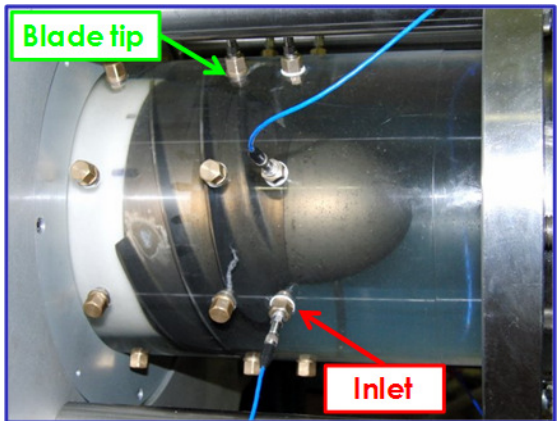

Figure 2. The transparent inlet section of the facility instrumented with piezoelectric pressure transducers.

The water pressure at the inlet of the test section can be adjusted by means of an air bag in the water tank, while the temperature regulation is obtained by means of a 5 kW electrical heater. A Silent Throttle Valve is used for the

variation of the pump load. Two electromagnetic flow meters (mod. 8732C by Fisher-Rosemount, range 0-100 l/s, accuracy 0.5% FS), mounted on the suction and discharge lines of the water loop, provide the measurement of the inlet and outlet flow rates. The inlet pressure is monitored by an absolute transducer positioned about one diameter upstream of the blade leading edges (Druck, model PMP 1400, 0÷1.5 bar operating range, 0.25% precision class), while a pair of redundant differential pressure transducers measure the pump pressure rise between the same inlet section and an outlet section positioned about two diameters downstream of the blade trailing edges (Kulite, model BMD 1P 1500 100, 0÷6.8 bar-d operating range, 0.1% precision class; Druck, model PMP 4170, 0÷1 bar-d operating range, 0.08% precision class). Photo cameras and high-speed video cameras can be used for visualization of the cavitating flow on the test article.

B. Test Article

The experimental campaign has been conducted on a four-bladed, tapered-hub, variable-pitch inducer, named DAPAMITO4. The test inducer, the main geometrical and operational parameters of which are reported in Table 1, is made of 7075-T6 aluminum alloy and has been designed using the reduced order model described in d'Agostino et al.[27,28].

The overall dimensions of this inducer have been chosen for installation and testing in the current CPRTF configuration. A moderate value of the blade loading (with a diffusion factor D = 0.38 as defined in d'Agostino et al.[27,28]) and a high solidity (σ_T = 2.25) have been chosen for reducing the leading-edge cavity and improving the suction performance. The value of the tip incidence-to-blade angle ratio $\alpha/\beta_b < 0.5$ has been selected with the aim of controlling the danger of surge instabilities at design flow under cavitating conditions. Figure 3, in particular, shows a front view of the inducer mounted in the test chamber of the facility, with the piezoelectric pressure transducers flush-mounted at a number of azimuthal locations.

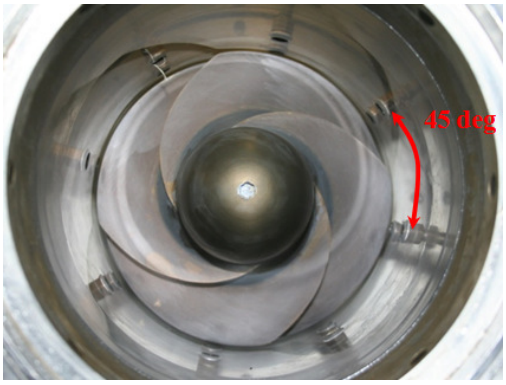

Figure 3. Frontal view of the DAPAMITO4 inducer inside the facility test chamber.

Table 1. Geometrical and operational parameters of the DAPAMITO4 inducer.

Design flow coefficient	[--]	Φ_D	0.070
Number of blades	[--]	N	4
Tip radius	mm	r_T	81.0
Inlet tip blade angle	deg	γ_{Tle}	81.10
Inlet hub radius (fully-developed blade)	mm	r_{Hle}	48.0
Outlet hub radius	mm	r_{Hte}	58.5
Mean blade height	mm	h_m	27.75
Axial length (fully-developed blade)	mm	c_a	63.5
Inlet hub radius	mm	r_{H1}	35.0
Axial length	mm	L	90.0
Diffusion factor	[--]	D	0.38
Ratio between tip incidence and blade angles	[--]	α/β_b	0.31
Tip solidity	[--]	σ_T	2.25
Incidence tip angle @ design	deg	α	2.74
Outlet tip blade angle	deg	γ_{Tte}	72.46

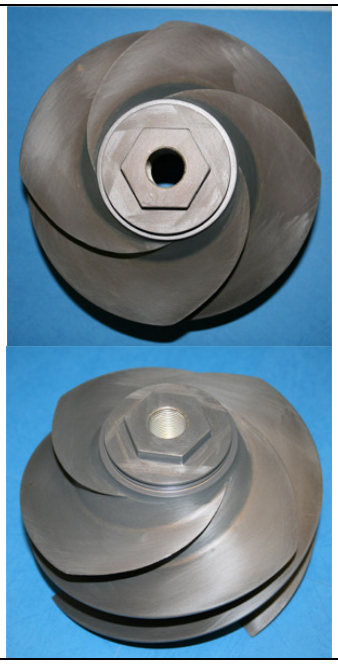

III. Results and Discussion

A. Noncavitating Performance and Hydraulic Efficiency

A first set of tests have been performed on the DAPAMITO4 inducer for the characterization of its noncavitating performance and hydraulic efficiency at two different water temperatures: 18.8 °C and 49.6 °C. The blade tip clearance for these tests was 2 mm, corresponding to 6.8% of the mean blade height. Figure 4 shows the noncavitating experimental curves in terms of the static head coefficient $\Psi = \Delta p / \rho \Omega^2 r_T^2$ and the hydraulic efficiency $\eta = Q\,\Delta p_t / (\tau\,\Omega)$ as functions of the flow coefficient $\Phi = Q / \pi \Omega r_T^3$.

In this case, the low pressure tap for the measurement of the static pressure rise has been located on the suction line, about 6 inducer diameters upstream of the blade leading edges, in order to eliminate the effect of inlet flow prerotation. The high pressure tap has been mounted on the discharge line at about 2.5 duct diameters downstream of the test chamber connection, because of the uncertainties in the influence of the exit flow swirl. Hence head measurements include the losses due to the flow diffusion from the inducer outlet into the test section and to the entrance in the discharge line. In order to evaluate the total pressure rise, some assumptions have been made both on the measured static pressure rise and the dynamic pressure at the exit of the inducer.

The torque τ has been directly measured by means of the rotating dynamometer, thereby by-passing the uncertainties associated with seal friction on the inducer shaft. The curves, obtained at a rotational speed of 1750 rpm and several temperatures of the liquid, confirm the independence of the test results on the flow temperature. The highest measured efficiency corresponding to the highest experimental flow coefficient (Φ = 0.052) is about 77%, in accordance with the typical values for this kind of machines (70÷80%).

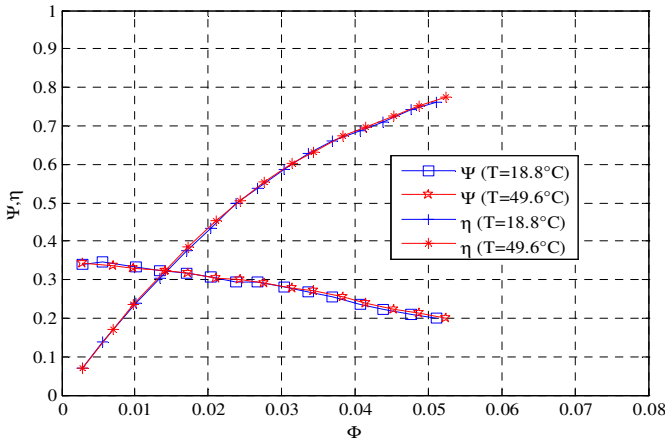

Figure 4. DAPAMITO4 inducer noncavitating performance and hydraulic efficiency at two different water temperatures.

B. Cavitating Performance

The cavitating performance of the inducer has been characterized in terms of the head coefficient as a function of the cavitation number $\sigma = (p_{in} - p_V) / \frac{1}{2}\rho\Omega^2 r_T^2$, at ambient temperature and rotating speed Ω =3000 rpm, for several values of the flow coefficient (84%, 80%, 76%, 71% and 63% of Φ_D). In the present case, the static pressure at inducer inlet has been used for the evaluation of the cavitation number.

Figure 5 (left) shows a comparison between the results obtained using two different test procedures, here indicated as "steady" and "continuous" experiments, and refers to a value of $c_{\%}$ (tip blade clearance to mean blade height ratios) equal to 2.7%. More in detail, the "steady" test results have been obtained by averaging the measurements over 2.4 s at fixed values of the flow coefficient and cavitation number, while the "continuous" test data have been taken keeping the flow coefficient and the pump rotational speed constant and gradually reducing the inlet pressure from atmospheric conditions to the minimum allowable value at a constant rate of about 3 mbar/s.

Figure 5 (right) illustrates the appearance of cavitation on the inducer at a flow coefficient equal to 76% of the design value and decreasing values of the cavitation number.

The performance curves show a "one step" shape under breakdown conditions, consisting of an intermediate head drop; as it will be shown in the next Sections, this phenomenon is associated to the occurrence of some forms of instabilities as the synchronous rotating cavitation.

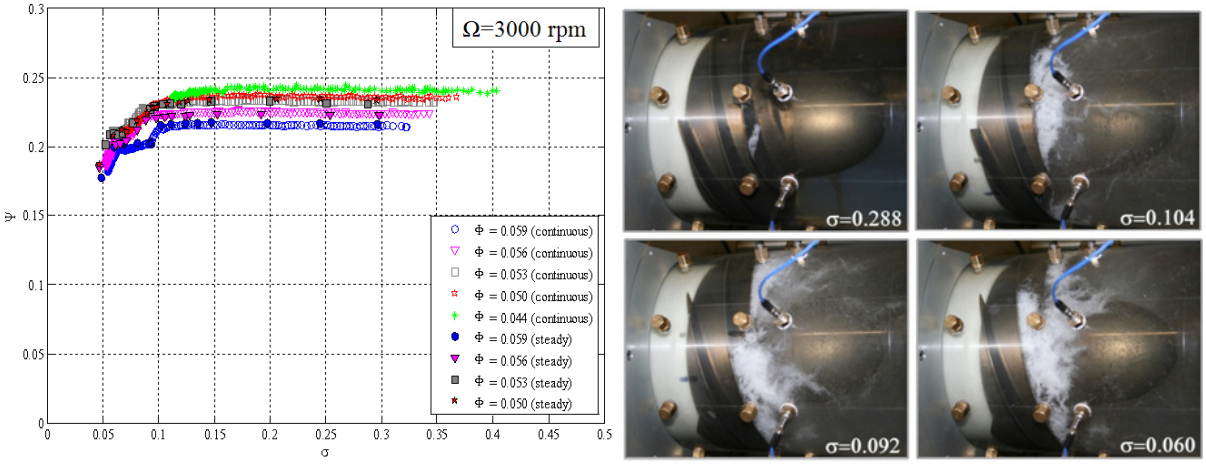

Figure 5. Cavitating performance of the DAPAMITO4 inducer at different flow coefficients (left) and appearance of cavitation in the inducer at different cavitation numbers, for $\Phi = 0.053$ (right). Data taken at ambient temperature $T = 15$ °C.

C. Flow Instabilities at Ambient Temperature

The instability analysis has been conducted for the same flow coefficients investigated during the cavitating performance characterization. The analysis is based on three steps: recognition of oscillating phenomena by the analysis of the pressure fluctuations in the inducer; definition of the most probable nature of the phenomena (axial or rotating and, in the second case, number of lobes and direction of rotation) by the analysis of the cross-spectra phases (φ) for different transducers couples at the same axial section (cross-spectra phases costantly close to 0 imply an axial phenomenon, cross-spectra phases close to $n \cdot \Delta\theta$, with n integer, imply a rotating phenomenon with n lobes); validation of previous points by the analysis of the coherence function γ_{xy} (only phenomena with $\gamma_{xy} > 0.8$ have been considered).

The tests illustrated in the present Section are referred to ambient temperature conditions ($T = 15$°C). Figures 6 and 7 show the waterfall plots obtained at $\Phi = 0.044$ and $\Phi = 0.056$, with $\Omega = 3000$ rpm; the inducer rotational frequency (50 Hz) and its harmonics ($n\Omega$) have been filtered. The orange boxes refer to the actual driving instabilities, the yellow ones to the non-linear interactions between the actual phenomena and the harmonics of the blade passage ($n\Omega$). Table 2 summarizes the flow instabilities detected on the DAPAMITO4 inducer at 0.8 mm clearance in terms of frequencies range, flow coefficients at which they have been observed, cavitation number range, typology of instability (rotating or axial) and number of lobes. Examination of the pressure fluctuations shows the occurrence of four different phenomena:

- The frequency denoted as *S (Surge)* is related to a 0-th order (axial) instability, as it can be inferred from cross-correlation analyses like the one presented in Figure 8. It appears at all the flow coefficients investigated in this experimental campaign.
- The frequency denoted as *BO (Backflow Oscillation)* appears only at the lowest flow coefficient. It is a single-cell, co-rotating instability (as shown in Figure 9) related to the backflow rotating speed (~0.2Ω), with similar characteristics to those illustrated by Tsujimoto et al. (2005)[31].
- The frequency denoted as *AO1 (Axial Oscillation 1)* is an axial instability which has been observed at all the flow coefficients. This phenomenon appears at high and intermediate cavitation numbers.
- Finally, the 4Ω - *BO* frequency refers to a three-cells co-rotating instability (likely due to a non-linear interaction between the blade passage frequency 4Ω and the backflow oscillation *BO*).

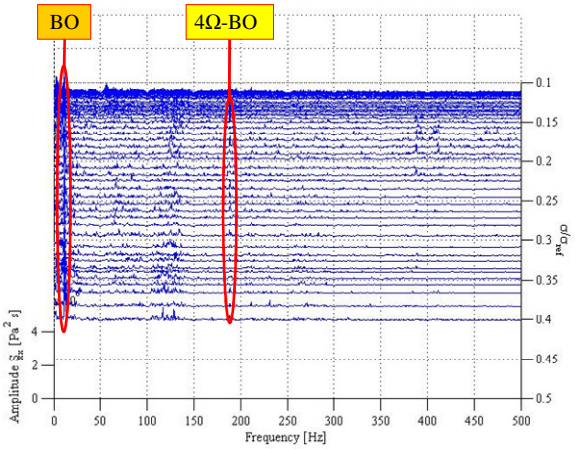

Figure 6. Waterfall plot of the power spectrum of the inlet pressure fluctuations on DAPAMITO4 inducer at Φ= 0.044 ($c_{\%}$= 2.7%, Ω= 3000 rpm, T= 15.0 °C), filtered for the $n\Omega$ frequencies.

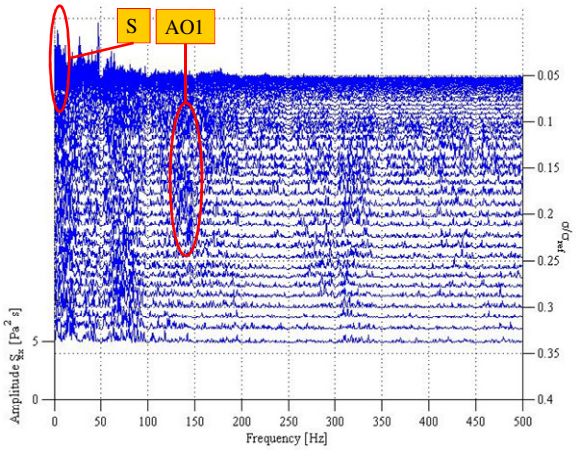

Figure 7. Waterfall plot of the power spectrum of the inlet pressure fluctuations on DAPAMITO4 inducer at Φ= 0.056 ($c_{\%}$= 2.7%, Ω= 3000 rpm, T= 15.0 °C), filtered for the $n\Omega$ frequencies.

Table 2. Flow instabilities detected on the DAPAMITO4 inducer ($c_{\%}$= 2.7%, Ω= 3000 rpm, T= 15.0 °C).

Instability I.D.	Frequency [Hz]	Φ	σ range	Type
S	1÷8.3	0.059	0.054÷0.079	Axial
		0.056	0.053÷0.093	
		0.053	0.058÷0.124	
		0.050	0.068÷0.122	
		0.044	0.113÷0.130	
BO	10.3÷11.7	0.044	0.113÷0.370	Rotating 1-lobe
AO1	127.4÷146.5	0.059	0.227÷0.293	Axial
		0.056	0.070÷0.247	
		0.053	0.107÷0.249	
		0.050	0.101÷0.171	
		0.044	0.118÷0.141	
4Ω - BO	188.5÷189	0.044	0.114÷0.130	Rotating 3-lobes

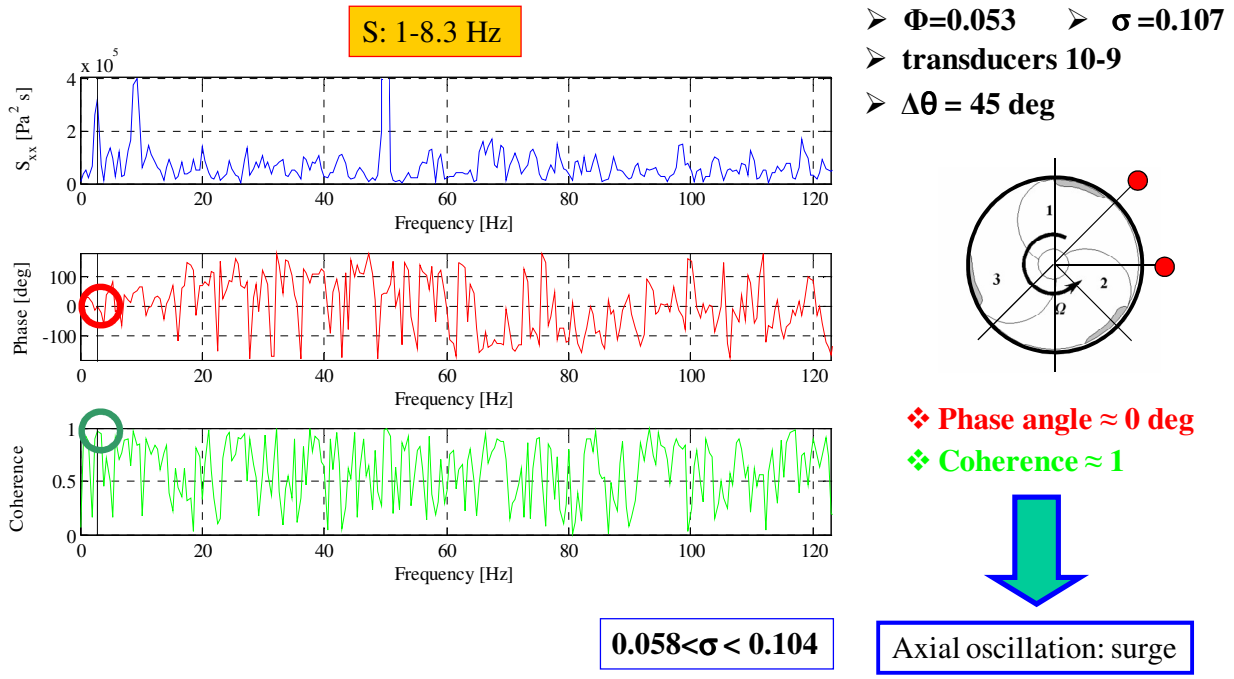

Figure 8. Amplitude and phase of the cross-spectral density and coherence function of the pressure signals of two transducers with 45° angular separation mounted at the inlet section of the DAPAMITO4 inducer (phenomenon= *S*, *Ω*= 3000 rpm, *T*=15.0 °C).

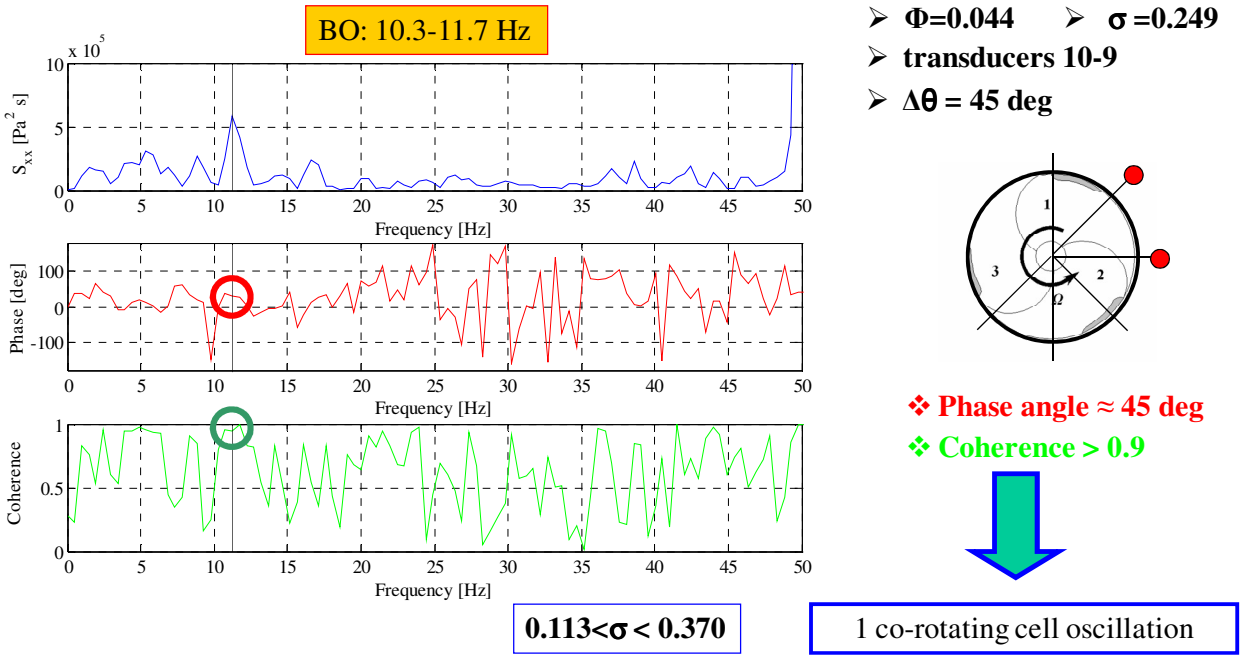

Figure 9. Amplitude and phase of the cross-spectral density and coherence function of the pressure signals of two transducers with 45° angular separation mounted at the inlet section of the DAPAMITO4 inducer (phenomenon= *BO*, *Ω* = 3000 rpm, *T*=15.0 °C).

D. Flow Instabilities at Higher Temperatures

Figures 10 and 11 show the waterfall plots obtained at Φ= 0.044 and Φ= 0.059 and a temperature of about 50 °C, with Ω = 3000 rpm; also in this case, the inducer rotational frequency (50 Hz) and its harmonics ($n\Omega$) have been filtered. The orange boxes refer to the actual driving instabilities, whereas the yellow ones are referred to the non-linear interactions between the actual phenomena and the harmonics of the blade passage ($n\Omega$).

Table 3 summarizes the flow instabilities detected in this case in terms of frequencies range, flow coefficients at which they have been observed, cavitation number range, typology of instability (rotating or axial) and number of lobes. Examination of the pressure fluctuations shows the occurrence of several different phenomena:

- The frequency denoted as *S (Surge)* is related to a 0-th order (axial) instability. It appears at all the investigated flow coefficients beginning at intermediate cavitation numbers, and has the same characteristics of the surge instability observed in the cold tests.
- The frequency denoted as *BO (Backflow Oscillation)*, as in the case of the cold tests, appears only at the lowest flow coefficient; it is a single-cell co-rotating instability related to the backflow rotating speed (~0.2Ω).
- The frequency denoted as *BVI1 (Backflow Vortices Instability 1)* appears to be related to a 3-lobes rotating phenomenon, typical of the backflow vortices instabilities. The phenomenon occurs at high and intermediate flow coefficients and is observed only at very low cavitation numbers (close to the head breakdown). The rotational frequency of the three lobes as a whole can be obtained by dividing the detected instability frequency by the number of lobes: *BVI1*/3≈10 Hz, which corresponds to the backflow rotating speed (~0.2Ω).
- The frequency denoted as *BVI2 (Backflow Vortices Instability 2)* appears to be related to a 2-lobes rotating phenomenon: even if the rotational frequency of the vortices system (*BVI2*/2 ≈ 20 Hz, about 0.4Ω) is higher than the typical one, this phenomenon has been associated to a backflow vortices instability.
- The frequency denoted as *AO1 (Axial Oscillation 1)* appears at all the flow coefficient except Φ=0.044: it is an axial oscillation and has the same characteristics of the similar one detected at ambient temperature.
- The other detected frequencies are likely to be caused by non-linear interactions between the phenomenona *BO*, *BVI1* and *BVI2* and the harmonics of the blade passage. The frequencies of these phenomena are 4Ω -*BVI2*,4Ω -*BVI1*,4Ω -*BO*, 4Ω +*BO*, 8Ω -*BO* and 8Ω +*BO*; the corresponding cross-correlation phases can be obtained by $\varphi(4\Omega\text{-}BVI2) = \varphi(4\Omega) - \varphi(BVI2)$, $\varphi(4\Omega\text{-}BVI1) = \varphi(4\Omega) - \varphi(BVI1)$, $\varphi(4\Omega\text{-}BO) = \varphi(4\Omega) - \varphi(BO)$, $\varphi(4\Omega\text{+}BO) = \varphi(4\Omega) + \varphi(BO)$, $\varphi(8\Omega\text{-}BO) = \varphi(8\Omega) - \varphi(BO)$, $\varphi(8\Omega\text{+}BO) = \varphi(8\Omega) + \varphi(BO)$.

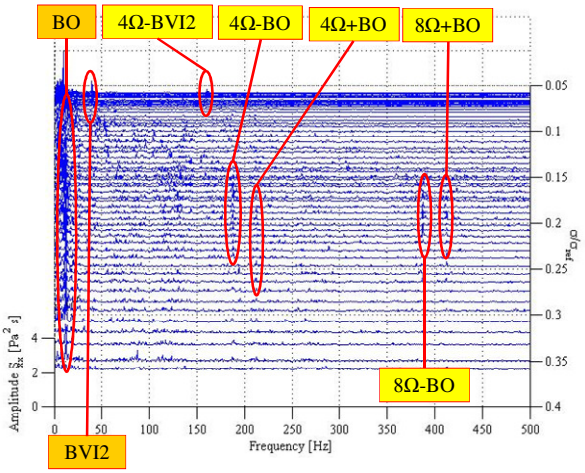

Figure 10. Waterfall plot of the power spectrum of the inlet pressure fluctuations on DAPAMITO4 inducer at Φ= 0.044 ($c_{\%}$= 2.7%, Ω= 3000 rpm, T= 49.7 °C), filtered for the $n\Omega$ frequencies.

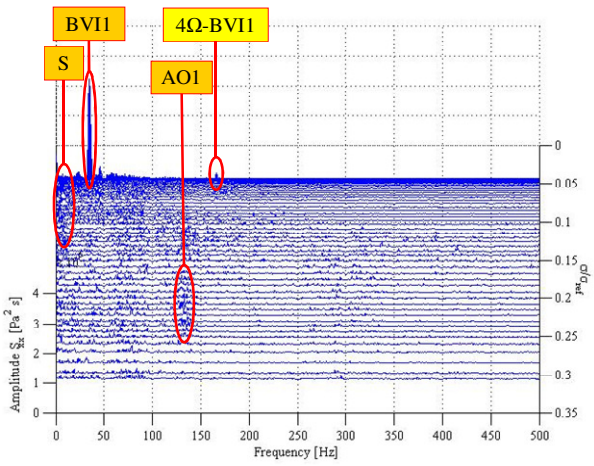

Figure 11. Waterfall plot of the power spectrum of the inlet pressure fluctuations on DAPAMITO4 inducer at Φ= 0.059 ($c_{\%}$= 2.7%, Ω= 3000 rpm, T= 50.0 °C), filtered for the $n\Omega$ frequencies.

Table 2. Flow instabilities detected on the DAPAMITO4 inducer ($c_{\%}$= 2.7%, Ω= 3000 rpm, T= 50.0 °C).

Instability I.D.	Frequency [Hz]	Φ	σ range	Type
S	1.5÷7.8	0.059	0.043÷0.121	Axial
		0.056	0.043÷0.187	
		0.053	0.046÷0.300	
		0.050	0.060÷0.184	
		0.044	0.059÷0.141	
BO	9.3÷12.7	0.044	0.060÷0.350	Rotating 1-lobe
BVI1	33.7÷36.6	0.059	0.043÷0.045	Rotating 3-lobes
		0.056	0.043÷0.047	
		0.053	0.045÷0.046	
BVI2	38.6÷42.5	0.050	0.067÷0.071	Rotating 2-lobes
		0.044	0.059÷0.076	
AO1	127.9÷138	0.059	0.121÷0.208	Axial
		0.056	0.094÷0.244	
		0.053	0.147÷0.265	
		0.050	0.170÷0.271	
4Ω - BVI2	155.3÷161.6	0.050	0.060÷0.071	Rotating 2-lobes
		0.044	0.059÷0.072	
4Ω - BVI1	166÷166.5	0.059	0.043÷0.044	Rotating 1-lobe
		0.056	0.043÷0.045	
		0.053	0.044÷0.045	
4Ω - BO	187.5÷191.9	0.044	0.141÷0.239	Rotating 3-lobes
4Ω + BO	212÷212.4	0.044	0.167÷0.266	Rotating 5-lobes
8Ω - BO	387.7÷388.2	0.044	0.161÷0.203	Rotating 7-lobes
8Ω + BO	406÷412	0.044	0.161÷0.203	Rotating 9-lobes

When water temperature is further increased, starting from a value of about 65 °C, a weak sub-synchronous rotating cavitation has been observed in addition to the previously described phenomena. This instability is a 1-lobe phenomenon rotating at a frequency between 0.8Ω and 0.95Ω, and occurs when the head coefficient begins to be affected by the cavitation (close to the breakdown conditions). The waterfall plot in Figure 12 shows a typical case of flow conditions under which this rotating cavitation instability has been detected while Figure 13 reports a magnification of the not-filtered waterfall plot highlighting how, at a certain cavitation number ($\sigma \approx 0.100$), the Synchronous Rotating Cavitation (SRC) at 50 Hz transforms into the sub-synchronous rotating cavitation (RC).

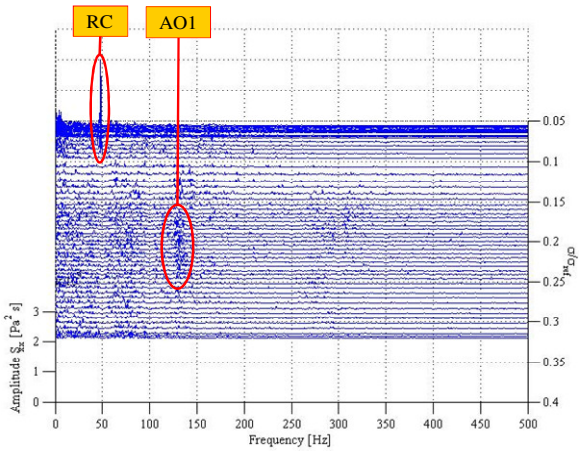

Figure 12. Waterfall plot of the power spectrum of the inlet pressure fluctuations on DAPAMITO4 inducer at Φ= 0.059 ($c_{\%}$= 2.7%, Ω= 3000 rpm, T= 64.8 °C), filtered for the $n\Omega$ frequencies.

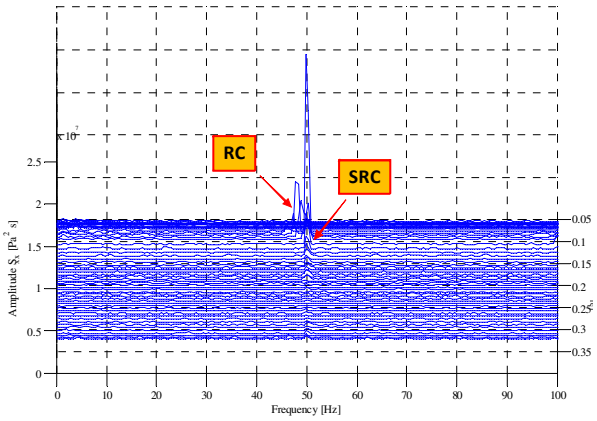

Figure 13. Magnification of the waterfall plot of the power spectrum of the inlet pressure fluctuations on the DAPAMITO4 inducer at Φ= 0.059 ($c_{\%}$= 2.7%, Ω= 3000 rpm, T= 64.8 °C).

E. Characterization of Synchronous Instabilities

Figure 14 shows the waterfall plot of the power spectrum of the inlet pressure fluctuations on the DAPAMITO4 inducer at Φ = 0.059 and ambient temperature: the harmonics of the blade passage, in this case, have not been filtered in order to eventually characterize the synchronous flow instabilities occurring on the pump. It can be observed that the peaks at Ω=50 Hz become significantly more evident in correspondence of the first head drop (see the cavitating performance curve reported on the *σ-Frequency* plane in the same plot).

The cross-correlation analysis confirmed that this phenomenon is a one co-rotating cell oscillation which can be classified as a "Synchronous Rotating Cavitation" (or "Steady Asymmetric Cavitation"). It is worth noticing that the maximum amplitude of oscillations is reached when the cavitating performance curve shows the "one step" shape under breakdown conditions, typical of this particular inducer.

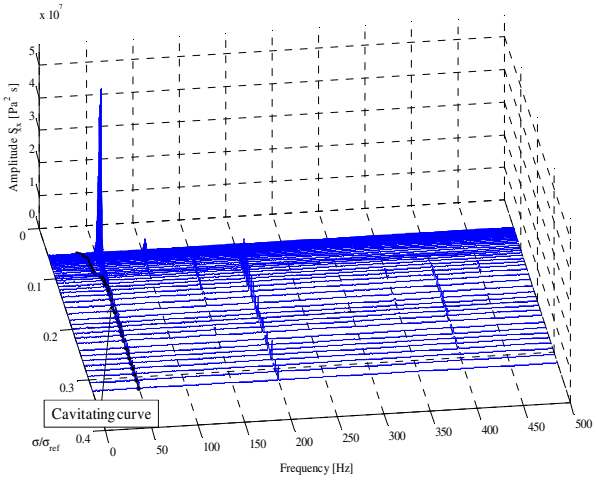

Figure 14. Non-filtered waterfall plot of the power spectrum of the inlet pressure fluctuations on DAPAMITO4 inducer at Φ= 0.059 ($c_{\%}$= 2.7%, Ω= 3000 rpm, T= 15.4 °C). The cavitating performance curve is represented as a black line on the *σ-Frequency* plane.

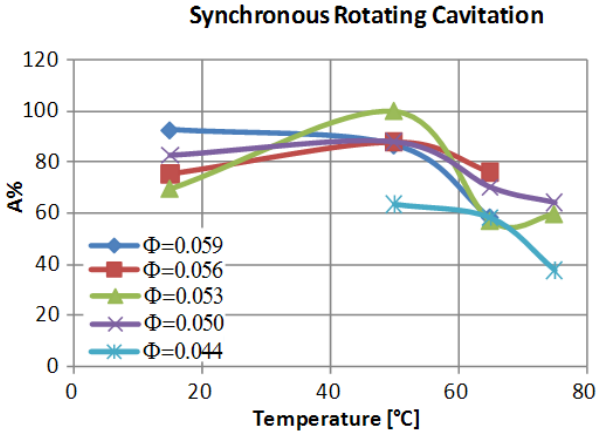

Figure 15. Amplitude (expressed as % of the maximum value, 15100 Pa) of the Synchronous Rotating Cavitation instability, as a function of the water temperature, at different flow coefficients ($c_{\%}$= 2.7%, Ω= 3000 rpm).

Concerning the amplitude of the Synchronous Rotating Cavitation oscillations, it is about one order of magnitude higher than the other non-synchronous instabilities. Analysis of the amplitude of oscillations at different water temperatures has shown that, as a general trend, it tends to decrease when temperature increases (see Figure 15). At the same time, looking at the cavitating performance curves, it has been clearly observed that the "one step" behavior becomes less and less evident when temperature increases. It can therefore be concluded that thermal cavitation effects have an influence on the flow instability itself (by reducing the amplitude of oscillations) as well as on the pump performance (by changing the shape of the performance curve and the extent of the "one step" behavior).

IV. Conclusions

A thorough experimental campaign has been conducted on a 4-bladed axial inducer, named DAPAMITO4, designed by means of a reduced-order model developed at Alta S.p.A. The cavitating and noncavitating performance of the pump have been characterized, as well as the flow instabilities acting on it at two different temperatures (15 °C and 50 °C). The following main considerations can be drawn from the results of the test campaign:

- The maximum hydraulic efficiency of the inducer is close to 80%.
- The cavitating performance of the inducer is characterized by a "one step" shape next to breakdown conditions, associated to the occurrence of a synchronous rotating instability (steady asymmetric cavitation).
- Only weak instabilities have been observed at ambient temperature, including a 0-th order surge and a backflow oscillation (characterized by one lobe rotating at 0.2 times the pump rotational speed).
- At higher water temperatures, together with the surge and the backflow oscillation, two different kinds of backflow vortices instabilities have been observed. In addition, at water temperatures equal to 65 °C or higher, a weak subsynchronous rotating cavitation phenomenon has been detected.
- The amplitude of the flow oscillations associated to the steady asymmetric cavitation generally tends to decrease when water temperature increases. Significant thermal cavitation effects can therefore be observed on both the flow instability extent and the cavitating performance of the inducer.

Acknowledgments

The present work has been supported by the European Space Agency under Contract No. 20081/06/NL/IA. The authors would like to express their gratitude to Dr. Johan Steelant of ESA-ESTEC, Prof. Mariano Andrenucci and Prof. Fabrizio Paganucci of the Aerospace Department, University of Pisa, Pisa, Italy, for their constant and friendly encouragement.

References

[1]Brennen C.E., "Hydrodynamics of Pumps", Concepts ETI, Inc. and Oxford University Press, 1994.

[2]Tsujjimoto Y., Kamijo K., Yoshida Y., "A Theoretical Analysis of Rotating Cavitation in Inducers", Journal of Fluids Engineereing, Vol. 115, No. 1, pp. 135-141, 1993.

[3]Kjeldsen, M., Effertz, M., Arndt, R. E. A., "Investigation of Unsteady Cavitation Phenomena", *Proceedings of US-Japan Seminar: Abnormal Flow Phenomena in Turbomachinery*, Osaka, Japan, Nov. 1-6, 1998.

[4]Higashi, S., Yoshida, Y. and Tsujimoto, Y., "Tip Leakage Vortex Cavitation from the Tip Clearance of a Single Hydrofoil", *CAV2001, International Symposium on Cavitation*, Pasadena, California, USA, June 20-23, 2001.

[5]Kubota, A., Kato, H., Yamaguchi, H. and Maeda, M., "Unsteady Structure Measurement of Cloud Cavitation on a Foil Section Using Conditional Sampling Technique", *Journal of Fluids Eng.*, Vol. 111, pp. 204-210, 1989.

[6]Tsujimoto, Y., Watanabe, S. and Horiguchi, H, "Linear Analyses of Cavitation Instabilities of Hydrofoils and Cascades", *Proceedings of US-Japan Seminar: Abnormal Flow Phenomena in Turbomachinery*, Osaka, Japan, Nov. 1-6, 1998.

[7]Callenaere, M., Franc, J. P. and Michel, J. M., "Influence of Cavity Thickness and Pressure Gradient on the Unsteady Behaviour of Partial Cavities", *3rd International Symposium on Cavitation*, Grenoble, France, April 7-10, 1998.

[8]Kawanami, Y., Kato, H., Yamaguchi, H., Tagaya, Y., and Tanimura, M., "Mechanism and Control of Cloud Cavitation", *ASME Journal of Fluids Engineering.*, Vol. 119, pp. 788-795, 1997.

[9]Sakoda, M., Yakushiji, R., Maeda, M. and Yamaguchi, H., "Mechanism of Cloud Cavitation Generation on a 2-D Hydrofoil", *CAV2001, International Symposium on Cavitation,* Pasadena, California, USA, June 20-23, 2001.

[10]Hashimoto T., Yoshida M., Watanabe M., Kamijo K. and Tsujimoto Y., "Experimental Study of Rotating Cavitation of Rocket Propellant Pump Inducers", *Journal of Propulsion and Power*, Vol. 13, N. 4., pp. 488-494, 1997.

[11]Zoladz, T., "Observations on Rotating Cavitation and Cavitation Surge from the Development of the Fastrac Engine Turbopump", *36th AIAA/ASME/SAE/ASEE Joint Propulsion Conference*, Huntsville, AL, USA, 2000.

[12]Ryan, R.S., Gross, L.A., Mills, D. and Michell, P., "The Space Shuttle Main Engine Liquid Oxygen Pump High-Synchronous Vibration Issue, the Problem, the Resolution Approach, the Solution", *30th AIAA/ASME/SAE/ASEE Joint Propulsion Conference*, Indianapolis, USA, 1994.

[13]Goirand, B., Mertz, A. L., Jousselin, F. and Rebattet, C., "Experimental Investigations of Radial Loads Induced by Partial Cavitation with Liquid Hydrogen Inducer", *IMechE*, C453/056, pp. 263-269, 1992.

[14]Tsujimoto, Y. and Semenov, Y. A., "New Types of Cavitation Instabilities in Inducers", *Space Launcher Liquid Propulsion: 4th International Conference on Space Launcher Technology*, Liege, Belgium, 2002.

[15]Uchiumi, M. and Kamijo, K., "Occurrence Range of a Rotating-Stall-Type Phenomenon in a High Head Liquid Hydrogen Inducer", *Proceedings of ISROMAC-12 - the 12th International Symposium on Transport Phenomena and Dynamics of Rotating Machinery*, Honolulu, Hawaii, USA, February 17-22, 2008.

[16]Tsujimoto, Y., "Simple Rules for Cavitation Instabilities in Turbomachinery", *CAV2001, International Symposium on Cavitation*, Pasadena, California, USA, June 20-23, 2001.

[17]Tsujimoto, Y., Yoshida, Y., Maekawa, Y., Watanabe, S. and Hashimoto, T., "Observations of Oscillating Cavitation of an Inducer", *ASME Journal of Fluids Engineering*, Vol. 119, pp. 775-781, 1997.

[18]Tomaru, H., Ugajin, H., Kawasaki, S., Nakano, M., "Suppression of Cavitation Surge in a Turbopump Inducer by the Backflow Restriction Step", *43rd AIAA/ASME/SAE/ASEE Joint Propulsion Conference*, Cincinnati, USA, 2007.

[19]Acosta, A. J., "An experimental study of cavitating inducers", *Proceedings of the Second ONR Symposium on Naval Hydrodynamics,* ONR/ACR-38, 533–557, 1958.

[20]Janigro, A. and Ferrini, F., "Inducer pumps. In Recent progress in pump Research", *von Karman Institute for Fluid Dynamics,* Lecture Series 61, 1973.

[21]Subbaraman, M. and Patton, M., "Suppressing Higher-Order Cavitation Phenomena in Axial Inducers", *CAV2006, 6th International Symposium on Cavitation*, Wageningen, The Netherlands, 2006.

[22]Kamijo, K., Yoshida, M. and Tsujimoto, Y., "Hydraulic and Mechanical Performance of LE-7 LOX Pump Inducer", *AIAA Journal of Propulsion and Power*, Vol. 9 (6): pp. 819-826, 1993.

[23]Imamura, H., Kurokawa, J., Matsui, J., and Kikuchi, M., "Suppression of Cavitating Flow in Inducer by J-Groove", OS-4-2006, *CAV 2003, 5th International Symposium on Cavitation*, Osaka, Japan, November 1-4, 2003.

[24]Horiguchi, H., Watanabe, S. and Tsujimoto, Y., "Theoretical Analysis of Cavitation in Inducers with Unequal Blades with Alternate Leading Edge Cutback: Part I- Analitical Methods and Results for Smaller Amount of Cutback", *Journal of Fluids Engineering*, Vol. 5, 2000.

[25]Yoshida, Y., Tsujimoto, Y., Kataoka, D., Horiguchi, H. and Wahl, F., "Effects od Alternative Leading Edge Cutback on Unsteady Cavitation in 4-Bladed Inducers", *Journal of Fluid Engineering*, Vol. 123, no. 4, pp. 762-770, Dec 2001.

[26]Shimura, T., Shimagaki, M., Watanabe, Y., Hasegawa, S. and Tanaka, S., "Cavitation Induced Vibration of LE-7A Oxygen Turpopump", OS-4-009, *CAV 2003, 5th International Symposium on Cavitation*, Osaka, Japan, November 1-4, 2003.

[27]d'Agostino, L., Torre, L., Pasini, A. and Cervone, A., "On the Preliminary Design and Noncavitating Performance of Tapered Axial Inducers", *ASME Journal of Fluids Engineering*, Vol. 130, Is. 11, November 2008.

[28]d'Agostino, L., Torre, L., Pasini, A., Baccarella, D., Cervone, A. and Milani, A., "A Reduced Order Model for Preliminary Design and Performance Prediction. Of Tapered Inducers: Comparison with Numerical Simulations", *44th AIAA/ASME/SAE/ASEE Joint Propulsion Conference*, Hartford, USA, 2008.

[29]Torre, L., Pace, G., Miloro, P., Pasini, A., Cervone, A., d'Agostino, L., "Flow Instabilities on a Three Bladed Axial Inducer at Variable Tip Clearance", 13th International Symposium on Transport Phenomena and Dynamics of Rotating Machinery, Honolulu, Hawaii, USA, April 2010.

[30]Rapposelli E., Cervone A. and d'Agostino L., "A New Cavitating Pump Rotordynamic Test Facility", *38th AIAA/ASME/SAE/ASEE Joint Propulsion Conference*, Indianapolis, USA, 2002.

[31]Tsujimoto, Y., Horiguci, H, Qiao, X, "Backflow from Inducer and its Dynamics", *ASME Fluid Engineering Division Summer Meeting and Exibition,* Houston, TX, USA, June 19-23, 2005.